Phys Chem Minerals (2001) 28: 445–454

ORIGINAL PAPER

C. I. Sainz-Díaz · J. Cuadros · A. Hernández-Laguna

Analysis of cation distribution in the octahedral sheet of dioctahedral 2:1 phyllosilicates by using inverse Monte Carlo methods

Received 13 July 2000 / Accepted 2 February 2001

Abstract An inverse Monte Carlo (MC) method was developed to determine the distribution of octahedral cations (Al^{3+}, Fe^{3+}, and Mg^{2+}) in bentonite illite–smectite (I–S) samples (dioctahedral 2:1 phyllosilicates) using FT–IR and ^{27}Al MAS NMR spectroscopies. FT–IR allows determination of the nature and proportion of different cation pairs bound to OH groups measuring the intensities of OH-bending bands. ^{27}Al MAS NMR data provide information about cation configuration because ^{27}Al MAS NMR intensity depends on Fe distribution. MC calculations based on FT–IR data alone show Fe segregation by short-range ordering (Fe clusters within 9 to 15 Å from a given Fe atom). Fe segregation increases with illite proportion. MC calculations based on IR and ^{27}Al NMR simultaneously yield similar configurations in which Fe clusters are smaller. The latter calculations fail to build appropriate cation distributions for those samples with higher number of illite layers and significant Fe content, which is indicative of long-range Fe ordering that cannot be detected by FT–IR and ^{27}Al MAS NMR. The proportion of Mg–Mg pairs is negligible in all samples, and calculations, in which the number of Mg atoms, as second neighbours, is minimised, create appropriate configurations.

Key words Dioctahedral 2:1 phyllosilicates · Smectite/Illite · Clays · Cation ordering · FT–IR · Al MAS NMR · Monte Carlo simulations

C. I. Sainz-Díaz (✉) · J. Cuadros[1] · A. Hernández-Laguna
Department of Earth Sciences and Environmental Chemistry,
Estación Experimental del Zaidín, CSIC,
Profesor Albareda 1, 18008 Granada, Spain
e-mail: sainz@eez.csic.es

Present address:
[1] Department of Mineralogy, National History Museum,
Cromwell Road, London SW7 5BD, UK

Introduction

Phyllosilicate minerals, and specifically smectite, have a wide range of chemical composition and different isomorphous cation substitutions in the octahedral and tetrahedral sheets. This fact generates a great diversity of these minerals in nature. In dioctahedral smectites, isomorphous substitution of Al^{3+} by Mg^{2+} in the octahedral sheet, or of Si^{4+} by Al^{3+} in the tetrahedral sheet, results in a net negative charge, which is balanced by cations in the interlayer space. Determination of the distribution of cations within the sheets is a complex problem, especially in the octahedral sheet, to which we refer in this paper. This type of study can be useful to understand natural processes, such as smectite to illite transformation, and to analyse how cation distribution affects lattice stability. Also, the industrial applications of smectite due to its valuable catalytic and adsorptive properties (e.g. as a barrier in nuclear waste and pollutant disposal repositories) make it of great interest to establish a firm theoretical understanding of their structure and behaviour.

Spectroscopic methods are especially useful for cation distribution analysis, since they probe local atomic environments and can detect short-range cation associations. Fourier transform infrared (FT–IR) spectroscopy of the vibrations of hydroxyl groups of 2:1 layer silicates has been used to assess octahedral cation distribution (Besson et al. 1987; Sainz-Diaz et al. 2000). The frequency of OH vibrations depends on the nature of the cations bonded to the OH group. ^{29}Si magic angle spinning (MAS) NMR has proven to be a sensitive probe of tetrahedral Al–Si cation ordering in aluminosilicate minerals. Different Si bands are detected depending on the neighbour cations. ^{27}Al MAS NMR spectroscopy can measure total intensities from octahedral Al in phyllosilicates. The paramagnetic character of Fe causes it to interact with the applied magnetic field and creates a field inhomogeneity that broadens the NMR signal and causes some signal loss of ^{27}Al MAS NMR. The Fe–magnetic field interaction occurs only within a short radius around the Fe atom, where the NMR

signal is lost. The resulting ^{27}Al NMR signal intensity depends on the effective Fe wipeout-sphere radius, which Schroeder and Pruett (1996) bracketed between 6 and 10 Å. Cuadros et al. (1999) tested different effective radii (in the range 6–8.5 Å) and found a minimum value of 7.5 Å. Thus, the total NMR signal from octahedral Al depends on the amount of octahedral Fe and its distribution. Increasing Fe segregation causes higher ^{27}Al NMR intensity because less Al atoms are close enough to Fe atoms for their NMR signal to be lost. Knowing the octahedral Fe and Al content in a sample together with the corresponding octahedral Al NMR signal intensity permits evaluation of how Fe is distributed in the octahedral sheet of phyllosilicates (Schroeder 1993).

Some of the previous studies assessing cation distribution in the octahedral sheet of phyllosilicates are the following. Using IR techniques, Slonimskaya et al. (1986) found that divalent and trivalent cations alternate within the octahedral sheet of celadonite, and Besson et al. (1987) showed that octahedral cation arrangement in the same mineral is not random and that Al^{3+} and Fe^{3+} tend to segregate from each other. Dainyak et al. (1992) performed Mössbauer analysis on a *trans*-vacant (i.e. vacancies in the octahedral sheet are in the M1 crystallographic position) glauconite and found that it presented celadonite- and illite-like domains in its octahedral sheet. Goodman et al. (1988) studied smectites by means of Mössbauer and electron paramagnetic resonance spectroscopies, finding that Fe was located in two different crystal-field environments that could be interpreted as either two phases, two crystallographic sites, or two different nearest-neighbour compositions. Morris et al. (1990) investigated Fe-bearing montmorillonites by means of ^{27}Al NMR and concluded that Fe was either segregated from Al in the octahedral sheet or present in a phase different from smectite. Grauby et al. (1991, 1993, 1994) synthesised smectites with different proportions of Al^{3+}, Mg^{2+} and Fe^{3+}. They studied how these cations arrange in the octahedral sheet using IR, and found that Al^{3+} and Fe^{3+} tend to mix rather than to segregate, Mg^{2+} and Fe^{3+} to segregate within the same layer, and Mg^{2+} and Al^{3+} to segregate, creating dioctahedral and trioctahedral layers. Schroeder (1993) studied shale illite–smectite (I–S) samples using ^{27}Al NMR and found that Fe mixes with Al in samples with low Fe content, but Fe segregates from Al in Fe-rich specimens. Drits et al. (1997) studied the isomorphous cation distribution in celadonites, glauconites and Fe-illites by IR, Mösbauer and EXAFS spectroscopies, together with simulations by probabilistic methods, finding certain short-range ordering. Muller et al. (1997) studied octahedral cation distribution of the Camp-Bertaux montmorillonite using XRD, EXAFS and FT–IR, and observed that Mg and Fe form clusters that segregate from Al.

However, it is very difficult to obtain an accurate description of the cation distribution by experimental methods alone, and it is in this respect that computer simulations can play a useful role in this type of studies. Monte Carlo (MC) simulations have been shown to be a powerful tool for the study of cation distribution and ordering in minerals. These methods have been used in aluminosilicates (Herrero and Ramírez 1992; Herrero 1993; Dove 1997; Dove and Heine 1996; Dove et al. 1996). In micas, the studies of Al and Si distribution in the tetrahedral sheet showed that no Al–Al pairs are found (Lowenstein rule) and that the number of Al–Si–Al groups is the smallest possible, but no long-range ordering was found (Herrero and Sanz 1991; Herrero et al. 1987; Vinograd 1995). However, cation distribution in the octahedral sheet of 2:1 layer silicates has been much less studied theoretically because of its higher complexity, arising from a wider variety of possible isomorphous substitutions.

In most of the ordering studies with MC simulations only two cations were considered. In this work, we studied the cation distribution by means of MC simulations for three species (Al, Fe and Mg) simultaneously. A previous study (Cuadros et al. 1999) of octahedral cation (Al, Fe and Mg) distribution in a series of I–S mixed-layer samples using FT–IR data and inverse Monte Carlo calculations, contrasted with ^{27}Al MAS NMR data, showed Fe segregation by short-range Fe ordering. Calculations for the most illitic specimens, however, suggested medium- or long-range Fe ordering. In this work, we extend the previous study to additional I–S samples, we further analyse the resulting distributions, and we present a method to determine cation distribution by fitting simultaneously FT–IR and ^{27}Al MAS NMR data.

Materials and experimental methods

The studied samples are bentonite I–S from several locations in North America and Europe with a wide range of illite composition (Table 1). A detailed description of the samples and their various analyses is published elsewhere (Cuadros and Altaner 1998a, b). Some samples of this series have been studied previously (Cuadros et al. 1999). In this work we complete the study of these samples and extend it to other samples of the series. Table 1 shows the octahedral composition of the studied samples determined by chemical analysis. The amount of Fe ranges from low (0.08 per unit cell) to fairly high (0.95). Based on the good match of structural formulae, all Fe was considered to be Fe(III).

For a detailed description of the experimental FT–IR study, see Cuadros and Altaner (1998a) and Cuadros et al. (1999), and for the NMR analysis see Cuadros et al. (1999). FT–IR data were obtained from the OH-bending bands in the region 917–780 cm^{-1}. The different bands correspond to OH linked to different cation pairs (M–OH–M). The relative intensities of these bands were transformed into metal abundances in the octahedral sheet assuming the same molar absorptivity for all M–OH–M bands (Table 1). This assumption is validated by previous work (Slonimskaya et al. 1986; Madejová et al. 1994; Besson and Drits 1997) and the good agreement between the chemical and IR-calculated metal abundances in the samples (Table 1). The RMS of the differences between chemical and FT–IR atom abundances is 0.074, which corresponds to 1.9% of total octahedral occupancy. Comparison of chemical and spectroscopical values by the Student's t statistic test showed that they are not significantly different. The illite and smectite components have a different charge in the tetrahedral sheet, which could affect the octahedral OH vibration frequencies. However, Sainz-Díaz et al. (2000) found recently that this effect is important in OH-stretching bands but negligible in OH-bending bands. The relative intensities of M–OH–M bands indicate the proportion of the different cation pairs in the octahedral sheet.

Table 1 Bentonite illite–smectite samples: composition of the octahedral sheet per unit cell [$O_{20}(OH)_4$] determined by chemical analysis and FT–IR, and octahedral ^{27}Al NMR intensity

Sample	Illite (%)[a]	Chemical analysis			FT–IR			NMR[b]
		Al	Fe	Mg	Al	Fe	Mg	
1-87	3	2.72	0.84	0.33	2.74	0.79	0.36	0.12
2-86	10	2.55	0.95	0.36	2.53	1.02	0.31	0.10
S-2	16	2.58	0.45	1.03	2.72	0.47	0.87	0.28
82-19g	30	3.34	0.29	0.51	3.33	0.32	0.45	0.51
R-80	45	3.05	0.27	0.68	3.03	0.32	0.65	0.41
83-1e	56	3.17	0.22	0.71	3.17	0.15	0.78	n.d.
82-2s	57	3.17	0.24	0.64	3.06	0.20	0.79	0.68
11b	60	3.17	0.22	0.58	3.08	0.21	0.69	0.51
14b	64	3.13	0.20	0.67	3.06	0.17	0.77	0.68
11a	68	3.27	0.19	0.54	3.11	0.21	0.69	0.69
26-171	71	3.30	0.13	0.59	3.22	0.31	0.49	n.d.
3-1	72	3.41	0.08	0.55	3.35	0.18	0.51	0.88
26-59	82	3.02	0.31	0.73	3.04	0.31	0.71	0.68
SWE-79	86	3.40	0.11	0.52	3.35	0.16	0.53	n.d.
82-36b	87	3.18	0.38	0.48	3.18	0.38	0.45	0.81
82-38	87	3.12	0.26	0.68	3.15	0.30	0.62	0.87
82-37c	90	3.10	0.08	0.82	3.12	0.14	0.75	0.88
82-32u	93	3.22	0.28	0.50	3.09	0.36	0.55	n.d.
WDH-25	93	3.34	0.23	0.47	3.39	0.18	0.48	n.d.
82-29	97	3.21	0.40	0.48	3.12	0.42	0.58	1.00

[a] Error $< 5\%$
[b] ^{27}Al MAS NMR intensity normalised to the highest value; n.d. not determined

The ^{27}Al MAS NMR intensities were measured, corrected for the octahedral Al content in the sample and normalised with respect to the highest value (Cuadros et al. 1999). The intensity values increase with illite content (Table 1; Fig. 3 in Cuadros et al. 1999). These intensities are relative values and are normalised to one of the highest values of the series.

Computational methods

The MC simulation was used to obtain octahedral cation distributions compatible with the proportion of cation pairs determined by FT–IR and with NMR experimental data. A computer program was specifically written for this study using standard FORTRAN 77 to run in a Digital Alpha workstation under Unix. The simulations were based on the MC technique using the Metropolis algorithm (Metropolis et al. 1953; Allen and Tildesley 1987), in the same way as Kirkpatrick et al. (1983) in their simulated annealing. Also, the simulations are similar to those performed in the reverse MC method used for determining the local structure of a disordered solid that best reproduces X-ray scattering (Uhlig et al. 1996), neutron scattering (Zotov and Keppler 1998) or ^{29}Si NMR spectra (Dove 1997).

Two types of experimental observables are considered: (1) the proportions of cation pairs ($Al^{3+}Al^{3+}$, $Al^{3+}Fe^{3+}$, $Al^{3+}Mg^{2+}$, $Fe^{3+}Fe^{3+}$, $Fe^{3+}Mg^{2+}$ and $Mg^{2+}Mg^{2+}$), obtained from the relative intensities of the FT–IR M–OH–M bands; and (2) the proportion of octahedral Al cations that are out of the inhibition radius of Fe cations and, hence, contribute to the NMR signal.

Our approach is to use a lattice model where the octahedral cations are in fixed positions forming a planar network with an intercationic distance of 3.04 Å (Lee and Guggenheim 1981). Owing to the dioctahedral nature of the samples, which implies that one out of three octahedral sites is vacant, the cations are arranged in the vertices of edge-sharing hexagons. A simulation cell of 5000 cations was used (corresponding to a supercell of $50 \times 25 \times 1$ unit cells of the mineral). To avoid artefacts at the boundaries of the simulation cell, periodical boundary conditions were applied to the system. The relative proportion of the Al, Fe and Mg cations is that given by the chemical analysis of each sample (Table 1). The starting configuration for the MC process was completely random, and was created by choosing randomly among Al, Fe and Mg and placing the atom at random in one of the 5000 sites of the simulation cell, which is originally empty. The random selection of cations takes into account the relative abundance of the three types of cations and those chosen in previous selections. This procedure is repeated until all sites are filled.

To analyse the cation distribution, the radial distribution function of each kind of cation was used. This is calculated as the summation, for all cations of one type, of the number of cations of the same type at different distances from one cation. This value is normalised with respect to the maximal values of cation concentration for each distance in our lattice and the proportion of each cation type.

IR-based MC simulation method

In order to know how closely the distribution of cations in the simulations resembles the experimental distribution, we define the quantity:

$$\alpha_{\mathrm{IR}} = \sum_{K}^{3} \sum_{K<L}^{3} f_{KL}[pp_{KL}(\mathrm{obs}) - pp_{KL}(\mathrm{calc})]^2 \quad (1)$$

$$\varepsilon_{\mathrm{IR}} = \sqrt{\frac{\alpha_{IR}}{n}} \quad (2)$$

where α_{IR} indicates the differences between experimental (FT–IR) and calculated values of proportions of cation pairs; obs and calc denote the experimental and calculated values, respectively; K and L indicate the cation (KL = AlAl, AlFe, AlMg, FeFe, FeMg and MgMg); pp_{KL} represents the proportion of each KL cation pair; f_{KL} is a weight factor for each kind of cation pair ($f_{KL} = 1$, except in some special case mentioned below); n is the number of all possible kinds of cation pairs (in our case, $n = 6$). The best distribution of the octahedral cations is that with the smallest value of ε. When all $f_{KL} = 1$, ε coincides with the root mean square (RMS) of the differences between observed and calculated distributions.

The MC method to approach a cation distribution compatible with the FT–IR data was as follows. In the original random distribution, two cations are selected randomly and their positions are exchanged if this action lowers the value of ε. If the value of ε increases, the atom positions are exchanged with a probability $\exp(-\varepsilon/\tau)$, where τ is a parameter chosen by the user. The link with the standard MC method is clear: ε plays the role of energy and τ plays the role of temperature. Each MC step is completed when all cations of the simulation cell have been exchanged. Steps are repeated until ε oscillates about a minimum mean value. Although all samples reached the equilibrium state before 1000 MC steps, 5000 MC steps were used in all samples to obtain good statistical results. Higher numbers of MC steps were tested in some samples (up to 5×10^6 MC steps), obtaining similar results. This method maximises the entropy in the octahedral cation distribution. When the simulation reaches equilibrium, the ε value of the calculated configurations oscillates slightly around the minimum value. At this point, the average value of the cation pair proportions from the last 100 configurations is calculated and this value is used in Eq. (1). This method is called inverse or reverse MC, but we will refer to it as MC for simplicity. The process is repeated at different values of τ as a simulated annealing method (Kirkpatrick et al. 1983). A slow reduction of τ is applied from an initial high value to the minimum one (six values from 1 to 10^{-5} in our case). This procedure reduces the probability that the minimisation leads the calculation to a false minimum of the function (local minimum) instead of the absolute minimum.

Charge dispersion constraint

Our MC simulation program can also calculate the IR-based configurations applying simultaneously a charge-dispersion con-

straint. The octahedral charge is produced by the Mg^{2+} substitution in our systems. A localised concentration of negative charge in the octahedral sheet would locally destabilise the structure and is most likely avoided in the mineral. Thus, charge dispersion was included in our simulations by dispersing the Mg^{2+} cations in the sheet. The simulations start from random distributions and fit simultaneously the FT–IR data with the constraint imposed. In a first step, we imposed the constraint that no MgMg pair exist (minimum Mg–Mg distance 5.25 Å). This was done by increasing the value of f_{MgMg} [f_{KL}, where KL = MgMg in Eq. (1)]. The reason for this is that increasing f_{MgMg} places more weight in the number of MgMg pairs for the calculation of $\varepsilon_{\mathrm{IR}}$. Since no MgMg pairs were found experimentally (see below), this procedure decreased the probability of finding such pairs from the calculated distributions. The f_{MgMg} values need to be finely tuned by increasing them slowly in successive calculations. In this process, RMS values (all $f_{KL} = 1$) were calculated for the same distributions and compared with the corresponding $\varepsilon_{\mathrm{IR}}$ ($f_{\mathrm{MgMg}} > 1$) values to control that they were similar. In the new distribution, however, Mg cations can still alternate as second neighbours and three Mg^{2+} can exist in the same hexagon of cations, which also represents a high concentration of negative charge. Thus, we introduced the additional constraint that the number of Mg–M–Mg groups must be minimal or, if possible, zero (minimum Mg–Mg distance of 6 Å). An additional hypothetical observable must be considered for this: the proportion of Mg cations as second neighbours (we call them Mg in *meta* position in the hexagon of cations by similarity with the relative positions in the hexagonal ring of benzene). Then, a new equation is used to fit the MC configurations to the FT–IR data and this new observable simultaneously:

$$\alpha_{\mathrm{Mg}meta} = f_{\mathrm{Mg}meta}[\mathrm{Mg}meta(\mathrm{obs}) - \mathrm{Mg}meta(\mathrm{calc})]^2 \quad (3)$$

$$\varepsilon_{\mathrm{IR-Mg}} = \sqrt{\frac{\alpha_{IR} + \alpha_{\mathrm{Mg}meta}}{n+1}}\ , \quad (4)$$

where α_{IR}, obs, calc and n have been defined above in Eqs. (1) and (2); Mg*meta* represents the proportion of Mg atoms as second neighbours; Mg*meta*(obs) is always zero; $f_{\mathrm{Mg}meta}$ is a weight factor that needs to be tuned in each case (similarly as described for f_{MgMg} above). In this case, the MC simulations are controlled by $\varepsilon_{\mathrm{IR\text{-}Mg}}$, which needs to be minimised.

MC simulation method based on FT–IR and NMR data

The following procedure was used to calculate MC configurations based on FT–IR and NMR data simultaneously. The simulations start from random distributions and fit the FT–IR and NMR data simultaneously. Our program calculates the intensity of the octahedral ^{27}Al NMR signal of each cation distribution, taking into account the intensity loss due to Fe. The ^{27}Al NMR signal intensity depends on the effective Fe wipeout-sphere radius. We used the minimal value of 7.5 Å for this radius determined by Cuadros et al. (1999). This Fe effect is constant for all ranges of illite composition of the I–S minerals. The intensity was calculated as a sum of all NMR-active Al atoms, by assigning a 0 value to Al atoms within the wipeout sphere of Fe cations and the intensity value of 1 to the contributing Al atoms. The signal intensity, for each sample, was averaged from the intensities of the last 100 MC configurations calculated after reaching the equilibrium. Therefore, we introduced a new observable and a new equation:

$$\alpha_{\mathrm{NMR}} = f_{\mathrm{NMR}}[\mathrm{NMR}(\mathrm{obs}) - \mathrm{NMR}(\mathrm{calc})]^2 \quad (5)$$

$$\varepsilon_{\mathrm{IR-NMR}} = \sqrt{\frac{\alpha_{\mathrm{IR}} + \alpha_{\mathrm{NMR}}}{n+1}} \quad (6)$$

where obs, calc and α_{IR} were defined for Eqs. (1) and (2); α_{NMR} controls the differences between experimental and calculated values of ^{27}Al MAS NMR data; and NMR is the relative intensity of the octahedral Al signal. NMR(obs) and NMR(calc) values need to be normalised to be compared because they are relative values. A rigorous normalisation implies dividing the observed and calculated intensities by those from a sample with no Fe, and hence, with a maximum intensity (intensities are previously normalised to octahedral Al content as indicated above). We did not have any Fe-free sample and we chose sample 82-37c, which has the lowest Fe and the second highest NMR intensity (together with 3-1; Table 1). This approximation can set some uncertainty in our α_{NMR} calculations because the intensity from sample 82-37c is affected by Fe distribution in it and, hence, this Fe distribution is affecting the calculated α_{NMR}. We can see this fact in Eqs. (5) and (6), where α_{NMR} will be zero for 82-37c. However, the magnitude of this possible uncertainty is small because the Fe content in 82-37c is very small (2% of octahedral occupancies). In fact, in previous work the IR-based MC configurations of 82-37c yielded an NMR intensity similar to the experimental value (Cuadros et al. 1999). Hence, this approximation is acceptable for our samples for comparative purposes. The nature and magnitudes of α_{IR} and α_{NMR} are different and we need to introduce a weight factor f_{NMR} to make them comparable. In this case, the MC simulations will be controlled by $\varepsilon_{\mathrm{IR\text{-}NMR}}$ and the best distribution will be that with the minimum $\varepsilon_{\mathrm{IR\text{-}NMR}}$ value.

We can also include the charge dispersion constraint in this MC simulation based simultaneously on FT–IR and NMR data. Thus, the calculation is controlled by $\varepsilon_{\mathrm{IR\text{-}Mg\text{-}NMR}}$ defined by:

$$\varepsilon_{\mathrm{IR-Mg-NMR}} = \sqrt{\frac{\alpha_{\mathrm{IR}} + \alpha_{\mathrm{Mg}meta} + \alpha_{\mathrm{NMR}}}{n+2}}\ . \quad (7)$$

Results

IR-based configurations

Initially, the proportion of cation pairs was obtained from the MC simulations by fitting only the FT–IR observables (considering only $\varepsilon_{\mathrm{IR}}$, Eq. 2) for each sample. Table 2 shows the proportions of cation pairs in the random configurations used as starting point and in the final MC distributions. Also in Table 2 the corresponding RMS values for the final configurations are included. The RMS values are within the range 0.3 to 3.6%, which is similar to the experimental error range. The main feature is that MC FeFe proportions are significantly higher than those from random distributions, indicating an important Fe segregation. The proportion of AlAl pairs in the MC configurations is close (in general, slightly lower) to those in the random distributions. AlFe and FeMg proportions are, in most cases, lower in the MC distributions. On the contrary, AlMg proportions are higher in the MC configurations. Finally, the MC MgMg proportions are lower than those from random distributions. All these results mean that the segregation of Fe produces an increase in AlMg pairs rather than a segregation of Al and Mg. Figure 1 shows some of the calculated configurations. Fe clustering is apparent in sample 82-2s by comparing the original random configuration (Fig. 1a) with the corresponding IR-based MC configuration (Fig. 1b). This effect is similar for samples with high content of Mg (sample S-2, Fig. 1c) and samples with high proportion of illite (sample 82-29, Fig. 1d).

One approach to determine quantitatively the distribution of cations is the radial distribution of each kind

Table 2 Relative proportion of octahedral cation pairs in the illite–smectite samples in the original random distribution and in the IR-based MC distribution. RMS values correspond to IR-based distributions

Sample	AlAl		AlFe		AlMg		FeFe		FeMg		MgMg		RMS
	Random	MC	Random	MC	Random	MC	Random	MC	Random	MC	Random	MC	
1-87	0.489	0.516	0.302	0.213	0.118	0.153	0.047	0.101	0.036	0.017	0.007	0.000	0.0079
2-86	0.436	0.469	0.325	0.266	0.123	0.117	0.061	0.090	0.046	0.047	0.009	0.011	0.0087
S-2	0.404	0.401	0.141	0.084	0.323	0.384	0.012	0.039	0.056	0.060	0.065	0.032	0.0195
82-19 g	0.651	0.649	0.113	0.101	0.199	0.214	0.005	0.013	0.017	0.012	0.015	0.010	0.0055
R-80	0.581	0.574	0.103	0.063	0.259	0.314	0.005	0.028	0.023	0.016	0.029	0.005	0.0051
83-1e	0.598	0.577	0.083	0.043	0.268	0.347	0.003	0.032	0.009	0.001	0.030	0.000	0.0137
82-2s	0.613	0.595	0.092	0.060	0.248	0.316	0.003	0.029	0.018	0.000	0.025	0.000	0.0292
11b	0.638	0.627	0.088	0.051	0.233	0.292	0.003	0.030	0.016	0.000	0.021	0.000	0.0214
14b	0.612	0.591	0.078	0.047	0.262	0.335	0.002	0.027	0.017	0.000	0.028	0.000	0.0200
11a	0.668	0.652	0.078	0.061	0.221	0.270	0.002	0.017	0.013	0.000	0.018	0.000	0.0359
26-171	0.674	0.659	0.053	0.065	0.241	0.257	0.001	0.000	0.009	0.000	0.022	0.019	0.0204
3-1	0.713	0.709	0.033	0.024	0.230	0.245	0.0004	0.0017	0.003	0.013	0.019	0.007	0.0109
26-59	0.554	0.531	0.114	0.088	0.268	0.336	0.006	0.025	0.028	0.015	0.032	0.004	0.0029
SWE-79	0.712	0.696	0.046	0.038	0.218	0.258	0.001	0.008	0.007	0.000	0.017	0.000	0.0075
82-36b	0.629	0.628	0.138	0.103	0.190	0.226	0.008	0.035	0.021	0.002	0.014	0.006	0.0038
82-38	0.591	0.581	0.098	0.081	0.257	0.293	0.004	0.015	0.021	0.017	0.028	0.013	0.0071
82-37c	0.601	0.571	0.031	0.036	0.318	0.372	0.0004	0.000	0.008	0.004	0.042	0.017	0.0103
82-32u	0.648	0.631	0.113	0.098	0.201	0.250	0.005	0.021	0.018	0.000	0.016	0.000	0.0196
WDH-25	0.683	0.688	0.094	0.048	0.192	0.228	0.003	0.031	0.013	0.005	0.014	0.000	0.0060
82-29	0.616	0.601	0.154	0.133	0.184	0.234	0.010	0.032	0.022	0.000	0.014	0.000	0.0240

of cation. Al, Mg and Fe radial distributions were calculated from one Al, Mg and Fe atom, respectively. For random configurations, the radial distributions of Al, Fe and Mg were uniform with only slight deviations from the mean value. The results are similar for all samples, with the only difference that the actual cation densities vary with the sample owing to the different cation contents. For IR-based MC configurations, the radial distribution of Al was similar to the random configuration (Fig. 2a). The Mg distribution is random only at distances higher than 5 Å, since no MgMg pair was found. Fe distribution shows a marked increase of cation density for short distances with respect to the random configuration, while the difference disappears at long distance. This indicates short-range ordering of Fe. This short-range ordering is more significant in samples with high illite content than in those with low illite content (Fig. 2b). The profiles of Fe radial distribution are similar for both groups, but illite-poor samples present ratios of 1.5–2.2 between the cation densities at short distance (3.04 Å) and long distance (>10 Å), whereas for illite-rich samples this ratio is 3.2–5. Also, illite-rich samples have Fe density values at long distance that are somewhat below those for the random configuration.

Charge dispersion

No MgMg pairs were detected in the FT–IR experimental results, which is consistent with previous data (Madejová et al. 1994). In half of the samples, the MC IR-based configurations did not show any such pairs either (Table 2) and the Mg radial distribution shows a negligible density at 3.04 Å (Fig. 2a). However, the other samples showed a small number of them that increases with Mg content, although the relative proportion of these MgMg pairs is lower than 3% in all the cases (Table 2). We corrected this small difference by means of our MC simulation method. Increasing slowly the value of the f_{MgMg} factor [f_{KL}, where $KL = \mathrm{MgMg}$ in Eq. (1)], the MC simulations can obtain configurations fitted to the IR data with a negligible proportion of MgMg pairs maintaining a low value of RMS similar to the previous configurations. However, the Mg radial distribution of these new configurations shows that the proportion of Mg at 5.25 Å is still high (Fig. 3a). We do not have experimental evidence about the existence of such groups, but they are likely to cause instability in the structure owing to local charge imbalance. We then used Eqs. (1), (3) and (4) where Mg *meta*(obs) was made zero in order to minimise the number of Mg–M–Mg groups in our calculated distributions. The f_{MgMg} ($KL = \mathrm{MgMg}$ in Eq. 1) and $f_{\mathrm{Mg}meta}$ (Eq. 3) factors were tuned up carefully in order to produce a maximal dispersion of Mg maintaining a minimal RMS with respect to the IR data. The introduction of this charge dispersion did not produce a significant effect on the Al and Fe distribution (Figs. 3b, 4a, b), and it generates a more stable and hence more realistic distribution. Figure 4a and b depicts the charge dispersion effect in the IR-based MC distributions for 14b, a sample with intermediate illite and Mg contents. A certain partial ordering can be observed for Mg distribution (Fig. 4b), in which Mg tends to form some superstructures (hexagons of Mg with a radius of 6.08 Å). The Mg radial distribution of these configurations shows no Mg at distances shorter than 6 Å and a high concentration of Mg at 6.08 Å (Fig. 3a). This concentration at 6.08 Å will depend on the Mg content in the sample.

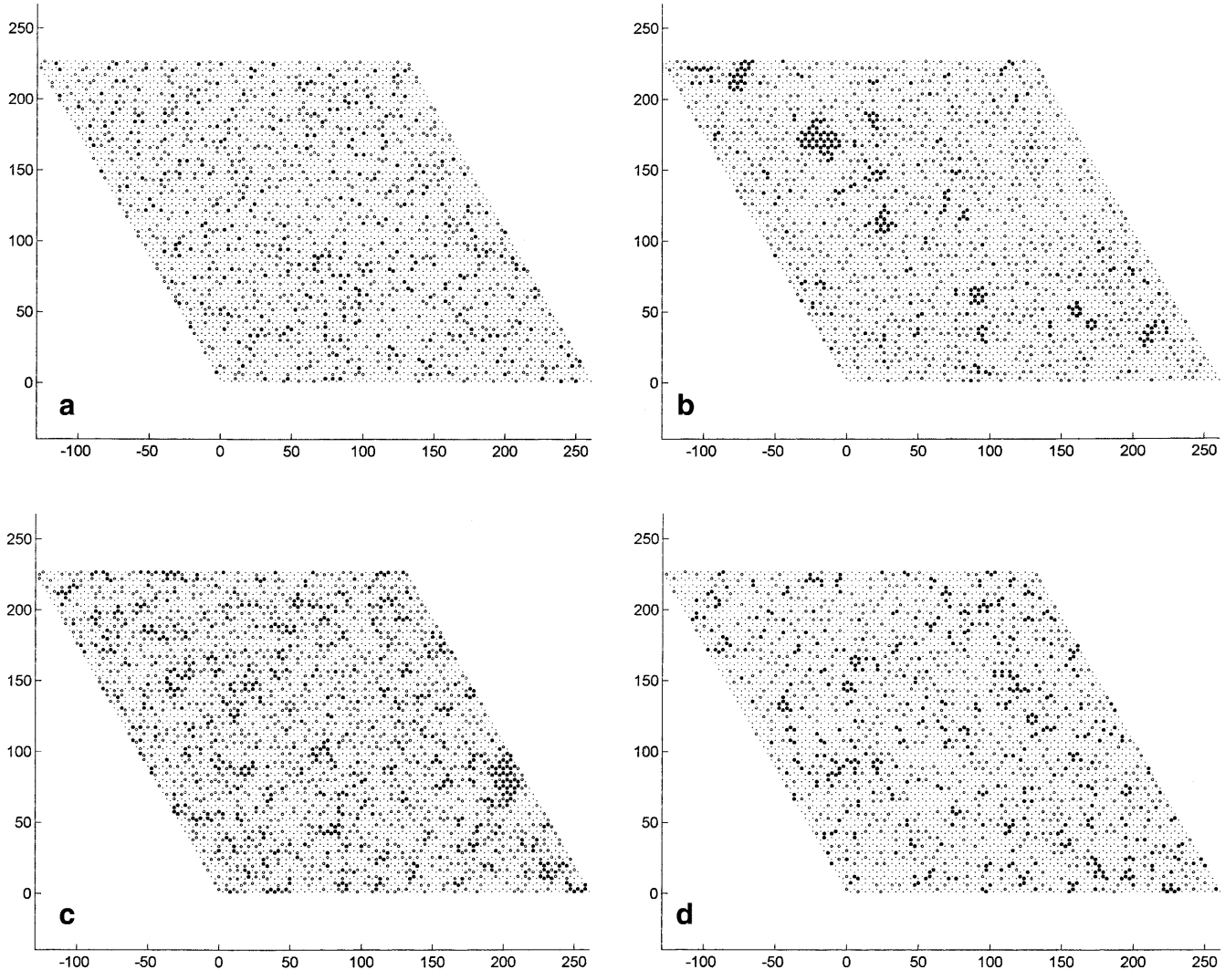

Fig. 1a–d Representations of octahedral cation distributions generated by MC simulations: random distribution of sample 82-2s (**a**), and IR-based configurations of samples 82-2s (**b**), S-2 (**c**) and 82-29 (**d**). Al (·), Fe (•), Mg (○)

MC simulations based simultaneously on FT–IR and NMR data

The inclusion of experimental NMR intensities as an observable in the MC simulations introduces spatial information of larger range because Fe atoms have a minimum wipeout (of NMR signal) sphere radius of 7.5 Å, as indicated above. The f_{NMR} factor in Eq. (5) was tuned carefully in order to obtain configurations fitted to the NMR data maintaining similar RMS values to those of the MC IR-based configurations. In Fig. 4a and c, the IR-based and the IR/NMR-based MC configurations of sample 14b are shown. Their comparison shows what can be observed for all samples: the size of Fe clusters is smaller in the IR/NMR-based configurations than in the IR-based ones. This is also shown by the diagrams of Fe radial distribution. Fe density decreases more rapidly with distance in IR/NMR-based configurations (Fig. 5a, b). This difference between IR- and IR/NMR-MC distributions becomes larger with increasing illite proportion in the I–S specimens (Fig. 5a, b). Nevertheless, Al and Mg radial distributions are similar for both kinds of calculations. No IR/NMR-based configuration with a low RMS value could be found for illite-rich samples whose Fe content is not low (82-29, 82-38, 82-36b and 26-59). These samples were found by Cuadros et al. (1999) to plot away from the general trend of Fe segregation in the same set of samples. Similar discrepancies were found by using a wipeout radius of 6 Å for the Fe effect, and these differences were higher with a radius of 8.5 Å. This different behaviour in these illitic samples indicates that Fe segregation follows patterns that are not detected by FT–IR and NMR analyses.

We also performed MC simulations using simultaneously FT–IR data, Mg dispersion, and NMR data (Eq. 7). We found configurations that fit all these variables maintaining RMS values similar to those of the MC IR-based configurations (Table 2) except for the samples mentioned above. In all cases, Fe distribution was similar to that without including a Mg dispersion factor (Fig. 5b).

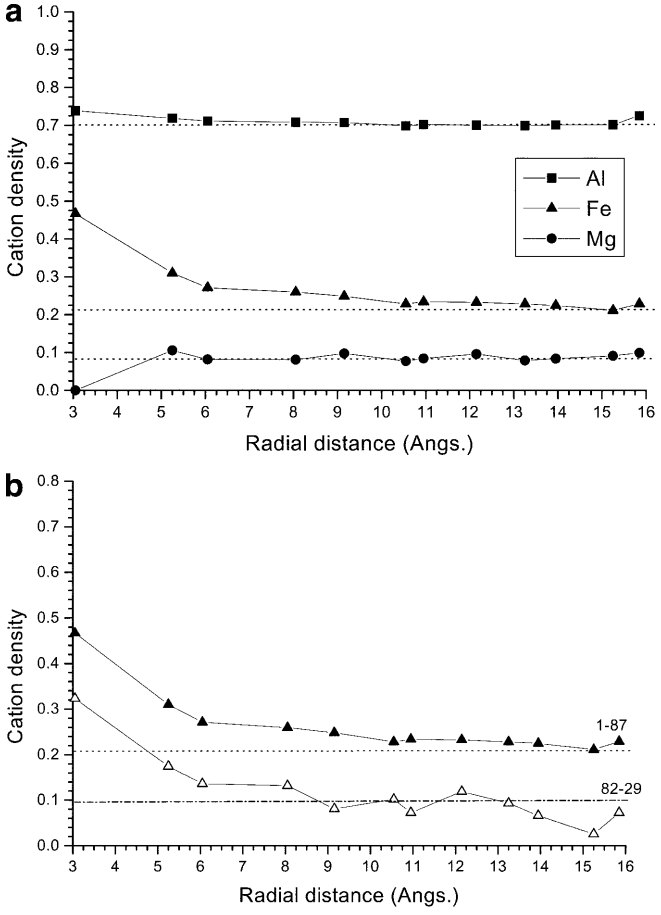

Fig. 2a, b Radial distribution of octahedral cations in the illite-smectite samples. **a** MC IR-based configuration of sample 1-87. **b** MC IR-based distribution of Fe in samples 1-87 (▲) and 82-29 (△) samples. The *dotted lines* represent the mean values of the corresponding random distributions for each case

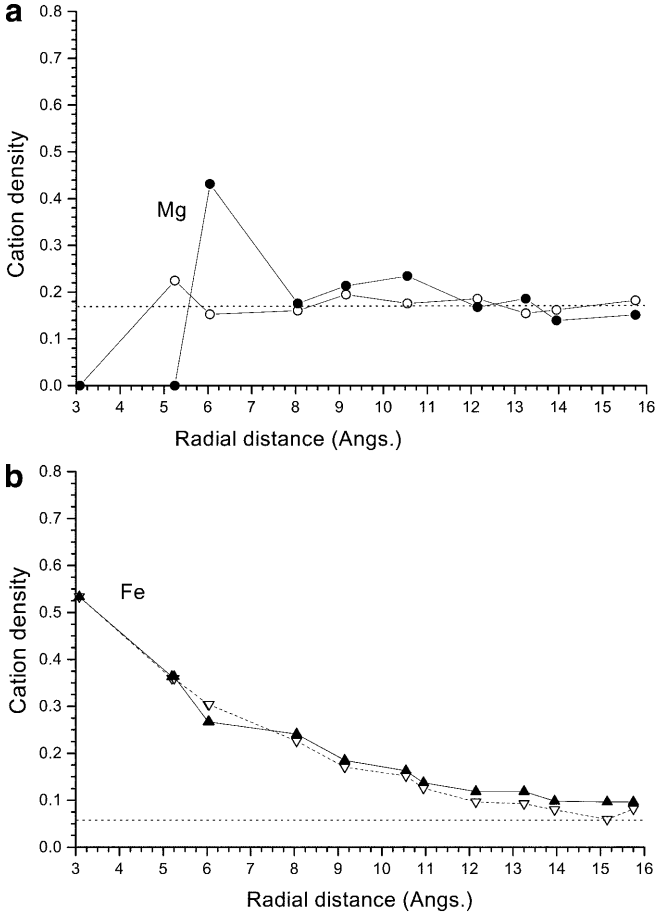

Fig. 3a, b Radial distribution of Mg (**a**) and Fe (**b**) in MC IR-based configurations of sample 14b with (*filled symbols*) and without (*open symbols*) Mg-dispersion constraints. The *dotted lines* represent mean values for a random distribution

Discussion

Our FT–IR and ^{27}Al MAS NMR data indicate that Fe segregates from Al and Mg in the analysed I–S series. ^{27}Al MAS NMR data also indicate that Fe segregation increases with illite content. Analysis of the IR-based MC configurations shows that Fe segregates by means of a short-range ordering because Fe clusters up to 9–15 Å (depending on the sample) from a given Fe atom. Further away, Fe concentration is approximately that in a random distribution. Of course, FT–IR data do not contain information on long-range ordering, and any model based only on this technique will very likely fail to recognise long-range ordering although it is present. This is what happens with samples 82-29, 82-38, 82-36b and 26-59. MC calculations generate configurations that are consistent with the IR data. Nevertheless, when NMR results are included in the calculation, the distributions cannot be correctly reproduced.

The Fe distribution in IR- and IR/NMR-based MC calculations is different in that Fe clusters are smaller in the latter. In Cuadros et al. (1999) only IR-based configurations were used and the calculated NMR intensities from these models were compared with those experimentally measured. The correlation was good with the exception of the above-mentioned samples, and the following equation was obtained:

$$I_{\mathrm{NMR}}(\mathrm{calc}) = 0.13 + 0.963 I_{\mathrm{NMR}}(\mathrm{exp}) \ , \qquad (8)$$

where I_{NMR} is the relative ^{27}Al MAS NMR intensity with respect to 82-37c; calc and exp represent the calculated values for the IR-based MC configurations and the experimental values, respectively. The intercept shows that in most samples the calculated NMR value is a little higher than the experimental one. This means that the size of the Fe clusters is overestimated in the IR-based MC configurations. This fact can be possible since the FT–IR data cannot control the medium and long-range ordering of cations. If the IR-based configurations tend to create Fe clusters larger than the actual ones, this difference is proportional to the size of clusters because the calculated-experimental ^{27}Al NMR intensity correlation is maintained. However, this difference can be reduced by means of MC simulations based on FT–IR

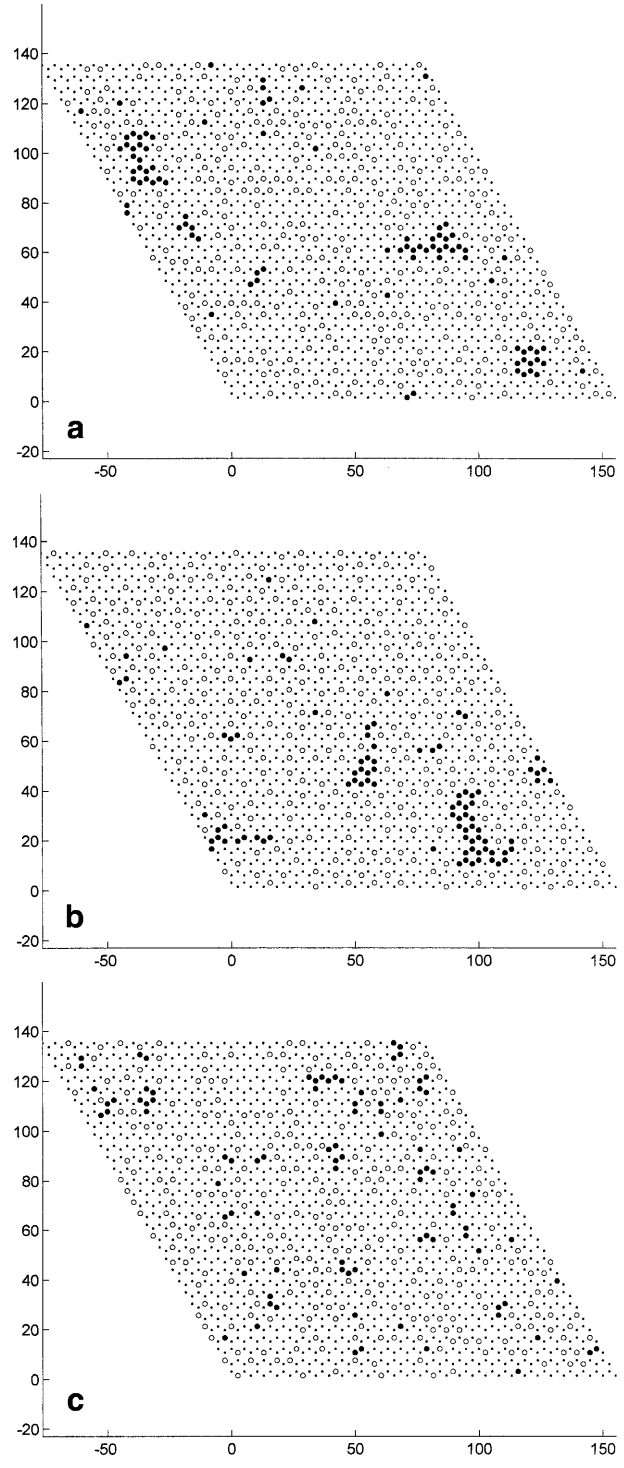

Fig. 4a–c IR-based MC configuration without (**a**), and with (**b**) charge dispersion constraints of sample 14b;(**c**) IR/NMR-based MC configuration of 14b. Al (·), Fe (●), Mg (○)

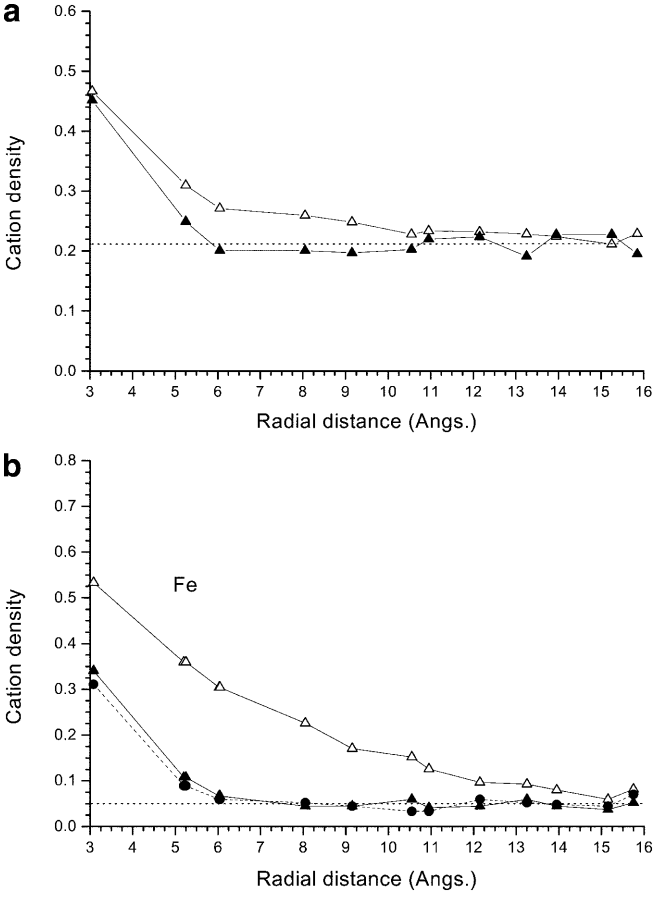

Fig. 5a, b Radial distribution of Fe in IR-based (*open symbols*) and IR/NMR-based (*filled symbols*) MC configurations for **a** sample 1–87 (3% illite) and **b** sample 14b (64% illite). *Filled circles* and *dashed line* in **b** correspond to a distribution with Mg dispersion constraints. *Dotted lines* represent mean values for random distributions

and NMR data simultaneously. In the NMR/IR-based MC configurations, the Fe clusters are smaller than in the IR-based configurations. Nevertheless, we cannot conclude that the NMR/IR-based MC configurations exactly represent the actual cation distributions because of the approximations that had to be included: (1) our observables give only short- and medium-range ordering information; (2) NMR is an indirect observable in our study and the intensities have been normalised with respect to a non-free Fe sample. However, the NMR/IR-based MC configurations are closer to the actual ones than the IR-based MC distributions. Further studies have to be performed in order to obtain more conclusive information of the long-range ordering of Fe in the I–S samples.

The illite-rich samples with a significant Fe content cannot be appropriately calculated because Fe segregation is produced by long-range ordering, which is not detected by FT–IR or NMR. To find the configurations resulting from this long-range ordering, we can create models with different patterns and see how they match with the different experimental data. Here is an example showing that different patterns produce different Fe radial distributions and that analysis of these distributions can be used to determine the type and proportion of configurations present. Figure 6 shows a chain-like and a globular Fe distribution. In the former, Fe density at 3.04 Å is high but that at 6.08, 9.12 and 10.9 Å is negligible. In the globular distribution, the concentration at

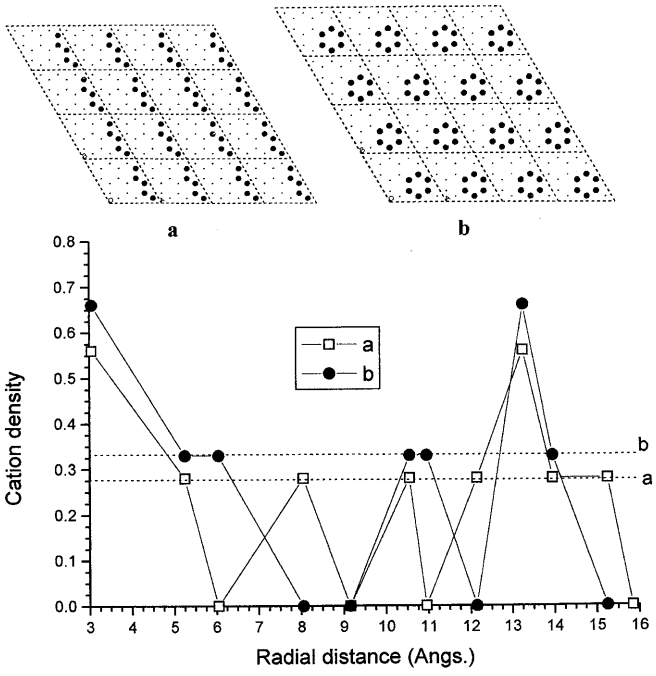

Fig. 6a, b Fe radial distribution of hypothetical models of ordered cation configurations (*dotted lines* represent mean values for random distributions). **a** Linear segregation in $Al_{2.88}Fe_{1.12}$ **b** Globular segregation in $Al_{2.68}Fe_{1.32}$ (per unit cell). Al (·), Fe (•)

3.04 Å is also high and no Fe is found at 8.1, 9.12 and 12.16 Å. The high values observed in both cases at 13.25 Å are artefacts caused by the selected distance between chains and hexagons in these models. Distributions of intermediate type between the two yield radial Fe densities that have also intermediate characteristics. Thus, Fe radial distribution can be related to ordering patterns. Fe contents in the given models ($Al_{2.88}Fe_{1.12}$ and $Al_{2.68}Fe_{1.32}$ per formula unit in chain-like and globular models, respectively) are higher than those in our samples and they cannot represent exactly the Fe distribution in them. Further development of this strategy can be used to analyse long-range ordering in these systems.

The minimisation of Mg–M–Mg groups is well "accepted" by the calculations. The configurations obtained with this constraint maintain the low RMS values and do not alter Fe distribution. Hence, although we do not have experimental data indicating such dispersion, we conclude that it occurs in the samples because unbalanced charge in the octahedral sheet is thus more disperse.

The overall picture shown by our I–S samples is that smectite illitisation causes an increasing Fe segregation in the octahedral sheet. This segregation is achieved by short-range ordering in specimens from low to intermediate illite content and by long-range ordering in illite-rich samples. According to this trend, cation ordering in the octahedral sheet changes gradually with illitisation. Cuadros and Altaner (1998b) found that these bentonite samples transformed from smectite to illite by means of a solid-state mechanism (i.e. there was no dissolution of the original smectite and precipitation of I–S). This poses the interesting question of how such a mechanism can provide for the observed structural changes. It seems that the solid-state transformation mechanism allows for atom reorganisation at a scale large enough to create long-range ordering. Further investigation to find clues to the way in which reaction fronts are created and propagated in this mechanism is desirable.

Conclusions

The combination of FT–IR, ^{27}Al MAS NMR and inverse MC simulations is a powerful and sensitive method to provide detailed information about the short-range distribution of cations in the octahedral sheet of phyllosilicates. IR-based MC simulations are able to generate configurations that reproduce the experimental IR data within experimental error. No MgMg pairs were observed by FT–IR in our I–S series. MC calculations using Mg dispersion constraints (minimum Mg–Mg distance of 6 Å) reproduced well the FT–IR data for all I–S samples and did not alter Fe distribution. Mg seems to order partially with the trend to form some superstructures. All I–S samples present Fe segregation, which is accompanied by an increase (with respect to a random distribution) of the proportion of AlMg pairs. Fe segregation increases with illite proportion. Analysis of Fe radial distribution showed that Fe segregation is caused by short-range ordering. MC calculations using simultaneously IR and NMR data showed configurations in which Fe clusters are smaller than those found in IR-based configurations. MC calculations failed to reproduce simultaneously IR and NMR data for illite-rich samples with significant Fe content. This suggests Fe segregation by long-range ordering, which cannot be detected by FT–IR and NMR data. Thus, smectite illitisation causes progressive Fe segregation in the octahedral sheet, first by short-range ordering and finally (> 80% illite) by long-range ordering.

Acknowledgements This work was supported by the DGES grant PB97-1205. The authors are grateful to Martin Dove and Michele Warren for their help and fruitful discussions, and to two anonymous reviewers for their insightful comments.

References

Allen MP, Tildesley DJ (1987) Computer simulations of liquids. Oxford Clarendon Press, Oxford

Besson G, Drits VA (1997) Refined relationships between chemical composition of dioctahedral fine-grained micaceous minerals and their infrared spectra within the OH-stretching region, part II: The main factors affecting OH vibrations and quantitative analysis. Clays Clay Miner 45: 170–183

Besson G, Drits VA, Daynyak LG, Smoliar BB (1987) Analysis of cation distribution in dioctahedral micaceous minerals on the basis of IR spectroscopy data. Clay Miner 22: 465–478

Cuadros J, Altaner SP (1998a) Compositional and structural features of the octahedral sheet in mixed-layer illite-smectite from bentonites. Eur J Mineral 10: 111–124

Cuadros J, Altaner SP (1998b) Characterization of mixed-layer illite-smectite from bentonites using microscopic, chemical, and X-ray methods: constraints on the smectite-to-illite transformation mechanism. Am Mineral 83: 762–774

Cuadros J, Sainz-Díaz C, Ramírez R, Hernández-Laguna A (1999) Analysis of Fe segregation in the octahedral sheet of bentonitic illite-smectite by means of FT–IR, ^{27}Al MAS NMR and reverse Monte Carlo simulations. Am J Sci 299: 289–308

Dainyak LG, Drits VA, Heifits LM (1992) Computer simulation of cation distribution in dioctahedral 2:1 layer silicates using IR data: application to Mössbauer spectroscopy of a glauconite sample. Clays Clay Miner 40: 470–479

Dove MT (1997) The use of ^{29}Si MAS-NMR and Monte Carlo methods in the study of Al/Si ordering in silicates. Geoderma 80: 353–368

Dove MT, Heine V (1996) The use of Monte Carlo methods to determine the distribution of Al and Si cations in framework aluminosilicates from ^{29}Si MAS NMR data. Am Mineral 81: 349–362

Dove MT, Thayaparam S, Heine V, Hammonds KD (1996) The phenomenon of low Al–Si ordering temperatures in aluminosilicates framework structures. Am Mineral 81: 349–362

Drits VA, Dainyak LG, Muller F, Besson G, Manceau A (1997) Isomorphous cation distribution in celadonites, glauconites and Fe-illites determined by infrared, Mösbauer and EXAFS spectroscopies. Clay Miner 32: 153–179

Goodman BA, Nadeau PH, Chadwick J (1988) Evidence for the multiphase nature of bentonites from Mössbauer and EPR spectroscopy. Clay Miner 23: 147–159

Grauby O, Petit S, Decarreau A (1991) Distribution of Al-Fe-Mg in octahedral sheets of synthetic smectites: study of three binary solid-solutions. Proc 7th Euroclay Conf. Dresden 441–446

Grauby O, Petit S, Decarreau A, Baronnet A (1993) The beidellite-saponite series: an experimental approach. Eur J Mineral 5: 623–635

Grauby O, Petit S, Decarreau A, Baronnet A (1994) The nontronite-saponite series: an experimental approach. Eur J Mineral 6: 99–112

Herrero CP (1993) Monte Carlo simulation of the Al, Si distribution in A-type zeolites. J Phys Chem 97: 3338–3343

Herrero CP, Sanz J (1991) Short-range order of the Si, Al distribution in layer silicates. J Phys Chem Sol 52: 1129–1135

Herrero CP, Ramirez R (1992) Energetics of cation ordering in the Faujasite framework: Monte Carlo simulations. J Phys Chem 96: 2246

Herrero CP, Gregorkiewitz M, Sanz J, Serratosa JM (1987) ^{29}Si MAS-NMR spectroscopy of mica-type silicates: observed and predicted distribution of tetrahedral Al–Si. Phys Chem Miner 15: 84–90

Kirkpatrick S, Gelatt CD Jr, Vecchi MP (1983) Optimization by simulated annealing. Science 220: 671

Lee JH, Guggenheim S (1981) Single crystal X-ray refinement of pyrophyllite-1*Tc*, Am Mineral 66: 350–357

Madejová J, Komadel P, Čičel B (1994) Infrared study of octahedral site populations in smectites. Clay Miner 29: 319–326

Metropolis N, Rosenbluth AW, Rosenbluth MN, Teller AH, Teller E (1953) Equation of state calculation by fast computing machines. J Chem Phys 21: 1087–1092

Morris HD, Bank S, Ellis PD (1990) ^{27}Al NMR spectroscopy of iron-bearing montmorillonite clays. J Phys Chem 94: 3121–3129

Muller F, Besson G, Manceau A, Drits VA (1997) Distribution of isomorphous cations within octahedral sheets in montmorillonite from Camp-Bertaux. Phys Chem Miner 24: 159–166

Sainz-Díaz CI, Timon V, Botella V, Hernández-Laguna A (2000) Isomorphous substitution effect on the vibration frequencies of hydroxyl groups in molecular cluster models of the clay octahedral sheet. Am Mineral 85: 1038–1045

Schroeder PA (1993) A chemical, XRD, and ^{27}Al MAS NMR investigation of Miocene Gulf Coast shales with application to understanding illite–smectite crystal chemistry. Clays Clay Miner 41: 668–679

Schroeder PA, Pruett RJ (1996) Fe ordering in kaolinite: insights from ^{29}Si and ^{27}Al MAS NMR spectroscopy. Am Mineral 81: 26–38

Slonimskaya MV, Besson G, Dainyak LG, Tchoubar C, Drits VA (1986) Interpretation of the IR spectra of celadonites and glauconites in the region of OH-stretching frequencies. Clay Miner 21: 377–388

Uhlig H, Hoffmann MJ, Lamparter H-P, Aldinger F, Bellissent R, Steeb S (1996) Short-range and medium-range order in lithium silicate glasses, part II: simulation of the structure by the reverse Monte Carlo method. J Am Ceram Soc 79: 2839–2846

Vinograd VL (1995) Substitution of $^{(4)}$Al in layer silicates: calculation of the Al-Si configurational entropy according to ^{29}Si NMR spectra. Phys Chem Miner 22: 87–89

Zotov N, Keppler H (1998) The structure of sodium tetrasilicate glass from neutron diffraction, reverse Monte Carlo simulations and Raman spectroscopy. Phys Chem Miner 25: 259–267